NASA Technical Memorandum 87351

Effect of Triangular Element Orientation on Finite Element Solutions of the Helmholtz Equation

Kenneth J. Baumeister
Lewis Research Center
Cleveland, Ohio

Prepared for the
1986 Winter Annual Meeting of the
American Society of Mechanical Engineers
Anaheim, California, December 7-12, 1986

NASA

EFFECT OF TRIANGULAR ELEMENT ORIENTATION ON FINITE ELEMENT SOLUTIONS OF THE HELMHOLTZ EQUATION

Kenneth J. Baumeister
National Aeronautics and Space Administration
Lewis Research Center
Cleveland, Ohio 44135

E-2734

ABSTRACT

The Galerkin finite element solutions for the scalar homogeneous Helmholtz equation are presented for no reflection, hard wall, and potential relief exit terminations with a variety of triangular element orientations. For this group of problems, the correlation between the accuracy of the solution and the orientation of the linear triangle is examined. Nonsymmetric element patterns are found to give generally poor results in the model problems investigated, particularly for cases where standing waves exist. For a fixed number of vertical elements, the results showed that symmetric element patterns give much better agreement with corresponding exact analytical results. In laminated wave guide application, the symmetric pyramid pattern is convenient to use and is shown to give excellent results.

NOMENCLATURE

A	constant coefficient
A_e	element area
B	constant coefficient
c	speed of propagation
D	domain of problem
$\{F\}$	global boundary condition vector
H	height of wave guide
i	$\sqrt{-1}$
$K_{i,j}^{(e)}$	local stiffness matrix component, Eq. (49)
$[K^{(e)}]$	local stiffness matrix
$[K]$	global stiffness matrix
k	wave number, Eq. (2)
L	length of wave guide
$N_j^{(e)}$	local element shape factor
$[N^{(e)}]$	local element shape matrix
n	total number of nodes
$\mathbf{n}$	unit outward normal
R	residual error
S	boundary line of domain D
t	time
W_i	global basis function $W_i(x,y)$
x	axial coordinate
y	transverse coordinate
$\partial/\partial n$	derivative in normal direction
∇^2	laplacian operator
∇	gradient operator
ζ_e	exit impedance, Eq. (11)
ϕ	potential $\phi(x,y)$
ϕ_i	nodal value of potential
$\phi^{(e)}$	value of potential in element, $\phi^{(e)}(x,y)$
$\{\phi\}$	global vector of nodal values ϕ_i
$\{\phi\}^{(e)}$	element vector of nodal values
ω	angular frequency

Superscripts

$\tilde{(\ )}$	approximate value of $(\ )$

(e) element value

* dimensional quantity

Subscripts

e exit or area

i index

j index

INTRODUCTION

The Helmholtz equation models many physical systems. In acoustics, the classic wave equation reduces to the Helmholtz equation which describes the propagation of harmonic pressure disturbances (1). Electromagnetic propagation in wave guides is also modeled by the solution of the Helmholtz equation (2). In fluid mechanics, a spectral approach to the Navier-Stokes equation also leads to the second order elliptic Helmholtz equation (3). The present paper is concerned with linear triangle finite element solutions to the Helmholtz equation. In particular, the optimum orientation of the triangle element pattern is examined for a number of typical boundary conditions associated with both acoustic and electromagnetic wave guides.

In acoustics and electromagnetic finite element modeling of the Helmholtz equation, first order linear triangular elements made their initial appearance in the late 1960's and early 1970's. Recently, higher order elements have supplanted the first order elements because of their higher accuracy. Nevertheless, first order elements continue to find use because they are simpler to understand and program (less chance for initial errors) and consequently they are an attractive starting point for a new research area. Many triangular patterns have appeared in the literature. In beam analysis, for example, the nonsymmetric pattern of triangles shown in Fig. 1(a) was shown to give less error than the symmetric pattern shown in Fig. 1(b) (4 p. 71). At the present time, however, the literature does not suggest which triangular element pattern might best be employed in the solution of the Helmholtz equation with boundary conditions typical of duct propagation problems.

Herein, the finite element solutions of the Helmholtz equation are obtained for plane wave propagation in a rectangular duct with a variety of linear triangle orientations. The correlation between the accuracy of the solution and the orientation of the linear triangles is examined for the following termination conditions: (1) no reflected wave at exit; (2) hard wall (infinite impedance); (3) potential relief (zero potential). Boundary conditions (1) and (2) are Neumann conditions and enter the problem as natural boundary conditions. On the other hand, the potential relief constraint enters the problem as a Dirichlet or forced boundary condition. Conditions (2) and (3) give rise to resonance inside the duct.

The first section of this paper presents the differential equation describing a scalar potential propagation in a wave guide. The second section presents model problems along with closed form analytical solutions which will later be compared to the finite element results. In the third section, the finite element formulation of the model problem is given. In the fourth section, finite element solutions and analytical solutions are compared for a number of triangular element patterns and termination boundary conditions for the proposed model problems. Finally, recommendations are made as to the advantages of the respective element orientations.

GOVERNING EQUATIONS AND BOUNDARY CONDITIONS

The governing differential equation describing the propagation of a harmonic scalar perturbation potential ϕ is the classic Helmholtz equation. The two-dimensional form of the homogeneous Helmholtz equation can be written as

$$\frac{\partial^2\phi}{\partial x^2} + \frac{\partial^2\phi}{\partial y^2} + k^2\phi = 0 \tag{1}$$

where k is the wave number representing a ratio of frequency to a propagation speed.

$$k = \frac{\omega}{c} \tag{2}$$

where all the variables are assumed dimensionless. The nondimensionalization begins with the speed of propagation c^*, frequency ω^* and dimensional potential ϕ^* and introduces their nondimensional equivalents. The superscript $(\ )^*$ denotes a dimensional quantity. The speed of propagation c^* is normalized with respect to c_o^* the velocity of propagation in a reference medium. The frequency ω^* is normalized by H^*/c_o^* where H^* is a characteristic length. The potential is normalized with respect to $c_o^*H^*$. In addition, lengths are scaled by H^*.

In wave guide propagation problems, the boundary conditions will depend on the type of source forcing the propagating or standing wave, the termination of the guide, and the properties of the walls of the wave guide. Typical boundary conditions for acoustic propagation can be found in Ref. 5 while the boundary conditions in electromagnetic theory are discussed in Ref. 2 (p. 67). The boundary conditions associated with the model problem under consideration in this paper will be presented in the next section.

MODEL PROBLEM

Finite element solutions of the Helmholtz equation will be determined for the two-dimensional boundary value problem shown in Fig. 2. In this problem, a uniform potential ϕ is assumed at $x = 0$,

$$\phi(0) = 1 \tag{3}$$

and the normal gradients of the potential are assumed zero at both the upper and lower walls,

$$\left.\frac{\partial\phi}{\partial n}\right|_{y=0} = \left.\frac{\partial\phi}{\partial y}\right|_{y=0} = 0 \tag{4}$$

$$\left.\frac{\partial\phi}{\partial n}\right|_{y=1} = -\left.\frac{\partial\phi}{\partial y}\right|_{y=1} = 0 \tag{5}$$

At the exit ($x = L$) of the wave guide, the three separate termination conditions shown in Fig. 2 will be considered. Their significance will be discussed shortly when the closed form analytical results are developed.

Closed Form Solution

Since the boundary conditions are uniform at the entrance and exit of the wave guide and are identical along the top and bottom of the guide, the scalar ϕ

will not depend on the y coordinate. Consequently, the governing Helmholtz equation reduces to

$$\frac{d^2\phi}{dx^2} + k^2\phi = 0 \tag{6}$$

which has a general solution of the form

$$\phi = Ae^{-ikx} + Be^{+ikx} \tag{7}$$

If the time dependence of the wave (neglected here) is assumed to be $e^{i\omega t}$, the Ae^{-ikx} represents a wave propagating in the positive x direction while Be^{ikx} represent a wave moving in the negative x direction (exactly the opposite would occur had a $e^{-i\omega t}$ time dependance been assumed). Details on the nature of wave propagation can be found in any text on acoustics (6).

Exit Terminations

Separate analytical and numerical solutions will be associated with each of the exit boundary conditions shown in Fig. 2. The significance of each of these conditions will now be discussed.

(1) No reflections at exit ($\zeta_e = 1$). Consider the case where waves only propagate to the right at $x = 1$. In this case,

$$B = 0 \tag{8}$$

and the exact analytical solution can be written as

$$\phi = e^{-ikx} = \cos kx - i \sin kx \tag{9}$$

The coefficient A has obviously taken on a value of unity to satisfy the entrance condition (3).

The exit termination boundary condition associated with this condition can be found by differentiating Eq. (9) and setting $x = L$:

$$\left.\frac{\partial\phi}{\partial x}\right|_L = -ike^{-ikL} = -ik\phi(L) \tag{10}$$

In wave propagation problems, it is customary and convenient to define an impedance of the form

$$\zeta_e \equiv \left.\frac{-ik\phi}{\frac{\partial\phi}{\partial x}}\right|_e \quad \text{or} \quad \left.\frac{\partial\phi}{\partial x}\right|_e = \frac{-ik\phi|_e}{\zeta_e} \tag{11}$$

For this definition, substituting Eq. (10) into Eq. (11) yields

$$\zeta_e = 1 \tag{12}$$

as shown as exit condition (1) in Fig. 2.

The specific problem to be considered herein will be for a k value of 2π. In this case, the real part of the analytical solution becomes

$$\text{Real}(\phi) = \cos 2\pi x \tag{13}$$

(2) Hard wall exit $\partial\phi/\partial x = 0$ ($\zeta = \infty$). The exit condition

$$\left.\frac{\partial\phi}{\partial x}\right|_e = 0 \tag{14}$$

along with condition (3) yield an equally simple solution

$$\phi = \frac{\cos k(L - x)}{\cos kL} \tag{15}$$

In this solution, both constants A and B have nonzero value. Consequently, the solution represented by Eq. (15) is a combination of forward (e^{-ikx}) and backward (e^{ikx}) traveling waves. A resonance reinforcement of the waves occurs when

$$kL = \frac{\pi}{2}, \frac{3\pi}{2}, \frac{5\pi}{2}, \ldots \tag{16}$$

The specific problem to be considered herein will again be for a k value of 2π. In this case, the analytical solution becomes

$$\phi = \cos 2\pi(L - x) \tag{17}$$

In contrast to Eq. (13), ϕ does not have any imaginary component, so the real designation is not required.

The term hard wall exit comes directly from acoustics. For a hard exit wall, the acoustic velocity represented by the gradient of the potential will be zero. In this case, substituting Eq. (14) into the definition for the impedance given by Eq. (11) yields

$$\zeta_e = \infty \tag{18}$$

Equation (18) will be conveniently employed in the finite element solutions to follow.

(3) Relief Exit ($\phi = 0$). The exit condition

$$\phi = 0 \quad \text{at} \quad x = L \tag{19}$$

along with condition (3) yields a solution of the form

$$\phi = \frac{\sin k(L - x)}{\sin kL} \qquad k > 0 \tag{20}$$

Again, because both constants A and B in Eq. (7) have nonzero values, the solution given by Eq. (20) represents the sum of forward and backward traveling waves. In this case, the resonance condition occurs when

$$kL = \pi, 2\pi, 3\pi, \ldots \tag{21}$$

For this boundary condition, three specific example problems will be developed. For the example shown in Fig. 2, where $L = 1$:

$$\text{(a) } k = 0 \quad \phi = 1 - x \tag{22}$$

$$\text{(b) } k = \frac{\pi}{2} \quad \phi = \sin\frac{\pi}{2}(1 - x) \tag{23}$$

$$\text{(c) } k = \frac{3\pi}{2} \quad \phi = \sin\frac{3\pi}{2}(1 - x) \tag{24}$$

In a sense, boundary conditions (2) and (3) in Fig. 2 are quite similar in that they both lead to standing wave patterns which are identical over certain regions. However, boundary condition (3) was introduced because it enters the finite element solution as a forced (Dirichlet) condition in contrast to boundary conditions (1) and (2) which enter the problem as natural boundary conditions. As pointed out clearly by Silvester and Ferrari (2, p. 11) these different formulations can significantly effect the accuracy of the

finite element results. In the weak formulation (7, p. 140) of the finite element equations the order of the differential equation is reduced using integration by parts (Green's vector identity). In this case the natural (Neumann) boundary conditions are not satisfied exactly but only in a certain mean-value sense which causes a contour integral in the finite element solution (to be presented shortly) to take on a prescribed value. The "strong" formulation, which enforces gradient boundary conditions exactly at a node (8), requires the use of Hermitian shape functions and is not considered herein.

FINITE ELEMENT THEORY

The finite element formulation is now generated by using the Galerkin method (9 to 11) to obtain an integral form of Eq. (1) over the whole (global) domain D shown in Fig. 2. A simplified and complete explanation of the Galerkin method is difficult to find in the literature. The presentation here is given in fair detail and is tutorial in nature.

System Discretization

The continuous domain D is first divided into a number of discrete areas staked out by the nodal points as shown in Fig. 1(a). Although the nodal points are shown evenly spaced in Fig. 1(a), the advantage of finite element theory is that it allows the placement of the nodes at any position desired. Next, the continuous potential $\phi(x,y)$ will be approximated (curve fitted) in terms of the nodal potential values ϕ_j located at x_j,y_j, see Fig. 1(b). The curve fit is required since we will integrate the governing Eq. (1) over the domain D shown in Fig. 2. This contrasts with the simplest form of finite difference theory (Taylor series) which usually only determines the potential at the lumped nodal points.

Global Weighted Residual Approach

In the classical weighted residual manner, the potential ϕ is curve fitted by expanding in terms of the nodal values $\phi_j(x_j,y_j)$ and a series of basis (shape) functions, such that

$$\tilde{\phi}(x,y) = \sum_{i=1}^{n} W_i(x,y)\phi_i = [W]\{\phi\} \qquad (25)$$

where the basis or weight functions $W_i(x,y)$ characterizes the spatial dependance of ϕ, and ϕ_j represents the unknown value of the potential ϕ at specific nodal points in the global region. The hat over the ϕ indicates that it is the approximate solution to ϕ. For example, ϕ_i would be associated with the potential value at the nodes shown in Fig. 1(a). In Fig. 1(a), the number of elements m has a value of 24, while the total number of nodes n has a value of 20. The nodes are numbered 1, 2, . . . n and the global vector $\{\phi\}$ represents the scalar values of the unknown potential ϕ at each node, such that in matrix form

$$\{\phi\} = \begin{Bmatrix} \phi_1 \\ \phi_2 \\ \phi_i \\ \phi_n \end{Bmatrix} \quad \text{or} \quad \{\phi\}^T = [\phi_1\ \phi_2 \cdots \phi_i \cdots \phi_n] \qquad (26)$$

The weight W_i has the property of being unity at node i and identical to zero at the other nodes. The weights W_i are all assumed to be known functions; consequently, we must guess some approximate form of W_i before the weighted residual approach can be applied. The values of $W_i(x,y)$ at points other than the nodes will generally be finite nonzero values. However, in the finite element (Galerkin) approximation for $W_i(x,y)$ to follow, throughout most of the domain the weight W_i is assumed zero not only at all other nodes but also at all values of x and y outside the element under consideration. This Galerkin approximation will considerably simplify the required integrations.

In general, substitution of Eq. (25) into the governing Eq. (1) and integrating over the domain D will not be equal to zero but will leave a residual error R.

$$\iint_D [\nabla^2\tilde{\phi} + k^2\tilde{\phi}]\, dx\, dy = R \qquad (27)$$

In accordance with the method of weighted residuals, the assumed basis functions W_i and the distribution of errors R are forced to be orthogonal (R = 0) within the region, such that

$$\left.\begin{aligned} &\iint_D W_1[\nabla^2\tilde{\phi} + k^2\tilde{\phi}]\, dx\, dy = 0 \\ &\iint_D W_2[\nabla^2\tilde{\phi} + k^2\tilde{\phi}]\, dx\, dy = 0 \\ &\qquad\vdots \\ &\iint_D W_i[\nabla^2\tilde{\phi} + k^2\tilde{\phi}]\, dx\, dy = 0 \\ &\qquad\vdots \\ &\iint_D W_n[\nabla^2\tilde{\phi} + k^2\tilde{\phi}]\, dx\, dy = 0 \end{aligned}\right\} \qquad (28)$$

Thus, there are n equations for the n nodal ϕ_i unknowns. In a direct analogy to the finite difference weighted residual control-volume formulation (12, pg. 30), each of the above equations can be thought of as a higher order difference approximation at the nodal point where W_i has a value of unity. Equations (28) can be written in compact form as

$$\iint_D W_i\left(\nabla\cdot\nabla\tilde{\phi} + k^2\tilde{\phi}\right) dx\, dy = 0$$

$$(i = 1, 2 \ldots, n \text{ equations}) \qquad (29)$$

By making use of Green's vector identity (integration by parts - 9, Eq. 9) and using the divergence theorem of Gauss (10, p. 79, Eq. 4.7(b)), Eq. (29) becomes

$$\iint_D (\nabla W_i\cdot\nabla\tilde{\phi} - k^2\tilde{\phi}W_i)dxdy - \int_S (W_i\nabla\tilde{\phi})\cdot\hat{n}\,ds = 0$$

$$(i = 1, 2 \ldots, n \text{ equations}) \qquad (30)$$

where n is the unit outward normal and S is the line integral around the global domain D as shown in Fig. 2.

In effect, we have reduced the order of the differential equation allowing us to employ the weak formulation of the finite element theory.
Thus, in the Galerkin finite element approximation to follow, simple class C_0 shape functions can now be used to approximate W_i. Across an element shown in Fig. 1 (a) for example, the class C_0 functions are only continuous in the dependent variable ϕ and are discontinuous in slope. As previously mentioned in the discussion of the boundary conditions, if Eq. (29) is treated directly, then Hermitian functions are required to approximate W_i (8). In these functions both the variable and its slope are continuous across a boundary.

Finite Element Approximation

Both the specifications of the global weighting functions W_i and the global integration over the whole domain D required by Eq. (30) are not practical. However, the integration can readily be performed by subdividing the domain into smaller elements A_e, defining the global shape function W_i in terms of the nodes of an individual element, integrating over an individual element and summing all the elements together.

Equation (30) is valid over the entire domain D shown in Fig. 2 or any subdomain A_e, as represented by the area of a small triangular element embedded in the region as depicted in Fig. 2. To begin the finite element aspect of the weighted residual method, the domain D is assumed to be divided into m elements defined by n nodes, as shown by the example in Fig. 1(a). In this case, Eq. (30) can be rewritten as

$$\sum_{e=1}^{m} \iint_{A_e} \left(\nabla W_i \cdot \nabla \tilde{\phi} - k^2 \tilde{\phi} W_i \right) dx\, dy - \int_S (W_i \nabla \tilde{\phi} \cdot \bar{n}\, ds) = 0$$

$$(i = 1, 2 \ldots, n \text{ equations}) \qquad (31)$$

Local Shape Factors

Each element is defined by the nodes around its perimeter. To represent the variation inside the elements of the field variable ϕ and its derivatives, local interpolation shape functions $N_i(x,y)$ for the linear triangle are written in both scalar and matrix form as

$$\tilde{\phi}(x,y) \approx \tilde{\phi}^{(e)}(x,y) = N_1^{(e)}(x,y)\phi_1^{(e)} + N_2^{(e)}(x,y)\phi_2^{(e)} + N_3^{(e)}(x,y)\phi_3^{(e)} = \sum_{j=1}^{3} N_j^{(e)} \phi_j^{(e)} = [N^{(e)}]\, \{\phi\}^{(e)} \qquad (32)$$

where $\{\phi\}^{(e)}$ is the vector of nodal values of ϕ for a general element e with subscripts 1, 2, and 3 representing the nodal positions, as shown in Fig. 2.

For example, for element 20 in Fig. 1(a), the vector $\{\phi\}^{(e)}$ would take on the form

$$\{\phi\}^{(e)} = \begin{Bmatrix} \phi_1 \\ \phi_2 \\ \phi_3 \end{Bmatrix} \Rightarrow \quad \{\phi\}^{(20)} = \begin{Bmatrix} \phi_{13} \\ \phi_{17} \\ \phi_{18} \end{Bmatrix} \qquad (33)$$

and the shape function

$$[N^{(e)}] = [N_1^{(e)} N_2^{(e)} N_3^{(e)}] \Rightarrow \quad [N^{(20)}] = [N_{13}^{(20)} N_{17}^{(20)} N_{18}^{(20)}] \qquad (34)$$

The form of the local shape matrix $[N^{(e)}]$ depends on the type of element used. For the linear triangle element employed herein, the known value of $N_j^{(e)}$ is simple in form and can readily be found in nearly every text on finite elements (2, Eq. 3.05). Like its global counterpart W_i, the local $N_j^{(e)}$ has the property of being unity at node j and zero at the other nodes in the triangle. For example, the magnitude of $N_1^{(1)}$ in element (1) is illustrated in Fig. 3(a). In this case, the magnitude of $N_1^{(1)}$ is represented by the height above the x-y plane. $N_j^{(e)}$ for other selected values are also seen in Fig. 3.

Notice that $N_{13}^{(e)}$ will have a nonzero value for elements (12), (13), (14), (19), (20), and (21). A superscript is required for $N_i^{(e)}$ to denote which element it resides, since the magnitude of this values the shape function at any x and y inside the element will depend on the location of the other corner nodes.

Replacing $\tilde{\phi}$ by $\tilde{\phi}^{(e)}$ in Eq. (31), the new governing equation becomes

$$\sum_{e=1}^{m} \iint_{A_e} \left(\nabla W_i \cdot \nabla \tilde{\phi}^{(e)} - k_i^2 \tilde{\phi}^{(e)} W_i \right) dx\, dy - \int_S (W_i \nabla \tilde{\phi}^{(e)} \cdot \bar{n} ds) = 0$$

$$(i = 1, 2, \ldots, n \text{ equations}) \qquad (35)$$

Galerkin Approximation

In general, the approximation for the $\tilde{\phi}$ distribution and the weight W_i can be different, as seen by now comparing Eqs. (25), (32), and (35) and, for example, as usually applied in weighted residual control-volume finite difference theory (12, pg. 32). In conventional finite element analysis as applied here, however, the weight function and the profile function are usually equated. The weight $W_i(x,y)$ is now approximated by multiple values of $N_i^{(e)}$. Adapting the Galerkin approximation to the more general weighted residual approach assumes that

$$W_i(x,y) = N_i^{(e)}(x,y) \qquad (36)$$

in all elements containing the node i. Approximation for W_i can be visualized by the pyramid-like shapes displayed in Fig. 3. For all elements which do not contain the node i, the weight W_i is assumed zero not only at all other nodes (as required by the general definition of W_i) but also at all values of x and y.

Recognizing that $N_i^{(e)}$ is zero for all elements not having the unknown ϕ_i associated with a

particular element, as shown in Fig. 3, the finite element Eq. (35) can be written in compact form as

$$\sum_{e=1}^{m} \iint_{A_e} \left(\nabla N_i^{(e)} \cdot \nabla \phi^{(e)} - k^2 \tilde{\phi}^{(e)} N_i \right) dA_e - \int_S (N_i \nabla \tilde{\phi}^{(e)} \cdot \bar{n} ds) = 0$$

$$(i = 1, 2, \ldots, n \text{ equations}) \qquad (37)$$

where N_i are the known shape factors (2, Eq. (3.05))

Surface Integral

The surface integral in Eq. (30) can be rewritten along the boundary in Fig. 2 as

$$\int_S W_i \nabla \tilde{\phi} \cdot \bar{n} ds = - \int_{FRONT} W_i \frac{\partial \tilde{\phi}}{\partial x} dy - \int_{BOT} W_i \frac{\partial \tilde{\phi}}{\partial y} dx + \int_{exit} W_i \frac{\partial \tilde{\phi}}{\partial x} dy + \int_{TOP} W_i \frac{\partial \phi}{\partial y} dx \qquad (38)$$

Since, $\partial\phi/\partial y$ is zero (Eqs. (4) and (5)) along the top and bottom for our model problem, Eq. (38) simplifies to

$$\int_S W_i \nabla \tilde{\phi} \cdot \bar{n} ds = - \int_{FRONT} W_i \frac{\partial \tilde{\phi}}{\partial x} dy + \int_{exit} W_i \frac{\partial \tilde{\phi}}{\partial x} dy \qquad (39)$$

or, utilizing the definition of impedance given by Eq. (11) yields

$$\int_S W_i \nabla \tilde{\phi} \cdot \bar{n} ds = - \int_{FRONT} W_i \frac{\partial \tilde{\phi}}{\partial x} dy - \frac{ik}{\zeta_e} \int_{exit} W_i \tilde{\phi} dy \qquad (40)$$

Employing $\phi^{(e)}$ and the Galerkin approximation, Eq. (36), Eq. (40) becomes

$$\int_S N_i^{(e)} \nabla \tilde{\phi}^{(e)} \cdot \bar{n} ds = - \int_{FRONT} N_i^{(e)} \frac{\partial \tilde{\phi}^{(e)}}{\partial x} dy - \frac{ik}{\zeta_e} \int_{exit} N_i^{(e)} \tilde{\phi}^{(e)} dy \qquad (41)$$

In terms of the general W_i in Eq. (40), both surface integrals would contribute to every element in the domain. However, with the Galerkin approximation the first term on the right hand side of Eq. (41) will only contribute when the nodal point i is on the right hand face. In Fig. 1(a), this would be points 1,2,3,4, and 5. For all other nodal positions, the value of N_i on the front face will be identical to zero by nature of the Galevkin approximation to W_i shown in Fig. 3. However, at points i on the front face boundary, ϕ (Dirichlet) boundary conditions are specified (forced). Thus, the i^{th} equation of Eq. (37) representing a boundary point will be discarded. The exact known answer will take its place;

$$\phi_i = 1 \qquad (42)$$

Thus, without loss of generality the first term or the right in Eq. (41) can be discarded, and

$$\int_S N_i^{(e)} \nabla \tilde{\phi}^{(e)} \cdot n ds = - \frac{ik}{\zeta_e} \int_{exit} N_i^{(e)} \phi^{(e)} dy \qquad (43)$$

For the relief exit condition, Eq. (19), the surface integral at the exit would also be discarded for the same reason.

The finite element equation for a general i node can now be written as

$$\sum_{e=1}^{m} \iint_{Ae} (\nabla N_i^{(e)} \cdot \nabla \tilde{\phi}^{(e)} - k^2 \phi^{(e)} \tilde{N}_i^{(e)}) dA_e + \frac{ik}{\zeta_e} \int_{exit} N_i^{(e)} \phi^{(e)} dy = 0$$

$$(i = 1, 2, \ldots, n \text{ equations}) \qquad (44)$$

EXAMPLE

The original global weighting function W_i associated with the i^{th} global node has now been assumed to be composed of the separate $N_i^{(e)}$ shape functions which reside in the local elements surrounding the i^{th} node, as shown in Fig. 3. For example, for $W^4 = N_4^{(e)}$, only the (5), (6), and (7) elements will contribute to the evaluation of the summation for the fourth node. Thus, for the grid and element notation of Fig. 1(a), the general Eq. (44) can be expanded into the form:

$\phi_1 = 1$ $\qquad i=1$

$\phi_2 = 1$ $\qquad i=2$

$\phi_3 = 1$ $\qquad i=3$

$\phi_4 = 1$ $\qquad i=4$

$\phi_5 = 1$ $\qquad i=5$

$$\sum_{e=1,2,9} \iint_{Ae} (\nabla N_6^{(e)} \cdot \nabla \tilde{d}^{(e)} - k^2 \tilde{\phi}^{(e)} N_6^{(e)}) dA = 0 \qquad i=6$$

$$\sum_{e=2,3,4,9,10,11} \iint_{Ae} (\nabla N_7^{(e)} \cdot \nabla \tilde{\phi}^{(e)} - k^2 \tilde{\phi}^{(e)} N_7^{(e)}) dA = 0 \qquad i=7$$

.

.

.

(equation continued on next page)

$$\sum_{e=22}^{24} \iint_{Ae} (\nabla N_{19}^{(e)} \cdot \nabla \tilde{\phi}^{(e)} - k^2 \tilde{\phi}^{(e)} N_{19}^{(e)}) dA + \frac{ik}{\zeta_e} \int_{Se} N_{19}^{(e)} \tilde{\phi}^{(e)} dy = 0 \quad i=19$$

$$\iint_{Ae} (\nabla N_{20}^{(24)} \cdot \nabla \tilde{\phi}^{(24)} - k^2 \tilde{\phi}^{(24)} N_{20}^{(24)}) dA + \frac{ik}{\zeta_e} \int_{Se} N_{20}^{(24)} \tilde{\phi}^{(24)} dy = 0 \quad i=20 \qquad (45)$$

In this example, the first five equations associated with Eq. (44) reduce to the forced Dirichlet boundary condition. The next two equations are typical of Eq. (44) applied to the central regions. No surface integrals appear since the value of N_i representing W_i in the domain D is zero outside the element containing i along the exit surface. Finally, when the i node coincides with the exit boundary, a surface integral contribution occurs, as in the last two equations. For i = 20, no summation is required since only one element area is associted with the final node. There are 20 equations associated with the 20 unknown values of the potential. Obviously because of the known boundary conditions, the equations could be reduced to fifteen.

Finite Element Equations

Expanding $\phi^{(e)}$ in terms of the weighting functions, Eq. (32) and neglecting the surface integrals for simplicity, Eq. (44) becomes

$$\sum_{e=1}^{m} \{\phi\}^{(e)} \iint_{A_e} \left[\nabla N_i^{(e)} \cdot [\nabla N^{(e)}] - k^2 N_i^{(e)} [N^{(e)}] \right] dA_e = 0$$

$$(i = 1, 2, \ldots, n \text{ equations}) \qquad (46)$$

where the $\{\phi\}^{(e)}$ local potential vector can be pulled outside the area integration since it does not depend on the area coordinates.

Equation (46) could in principle be evaluated for each i to yield a set of n simultaneous equations for the n unknown values of ϕ_j, as in Eq. (45). However, this approach is not readily implemented on a digital computer. Rather, each element is treated independently and the contributions of a single element to all the equations in Eq. (46) are determined simultaneously from the following:

$$\{\phi\}^{(e)} \iint_{A_e} \left[\nabla N_j^{(e)} \cdot [\nabla N^{(e)}] - k^2 N_j^{(e)} [N^{(e)}] \right] dA = 0$$

$$(j = 1, 2, 3) \qquad (47)$$

In contrast to the i subscript of Eq. (46) for all the nodes in the global domain, here the subscript j sums only the three nodes of a particular element. In compact standard finite element form, Eq. (47) can be written as

$$[K^{(e)}] \{\phi\}^{(e)} = 0 \qquad (48)$$

where

$$K_{i,j}^{(e)} = \iint_{A_e} \left[N_{ix}^{(e)} N_{jx}^{(e)} + N_{iy}^{(e)} N_{jy}^{(e)} - k^2 N_i^{(e)} N_j^{(e)} \right] dx\, dy \qquad (49)$$

For triangular elements, the evaluation of Eq. (49) is quite simple and presented in many texts (11, p. 149, Eq. 8.42 for the first two terms and p. 45 for the last term). The surface integral is evaluated in a similar manner.

Using the standard finite element procedures (11), the elemental Eqs. (48) can be assembled into Eq. (46) and the boundary conditions applied to yield the following global set of simultaneous equations which we can solve to obtain the unknown nodal potentials:

$$[K]\{\phi\} = \{F\} \qquad (50)$$

Here, the column vector {F} contains boundary condition information and the global stiffness matrix [K] is the sum of the known local stiffness matrices $[K^{(e)}]$. The solution of Eq. (50) by a banded Gauss solver yields ϕ_j. Except for a few minor modifications, a complete fortran listing of the banded solver can be found in Ref. 13, program 16, page 64.

Next, the solutions of Eq. (50) for a number of element discretization patterns and boundary conditions will be compared to the analytical solutions.

RESULTS AND COMPARISONS

Finite element solutions for a variety of exit terminations will now be compared to the closed form analytical solutions presented earlier. Four distinct triangular grid orientations will be considered.

Nonsymmetric Grid

The nonsymmetric grid shown in Fig. 4 was used to calculate wave propagation without reflection at the exit, Eq. (13). This grid orientation is labeled nonsymmetric since views looking from the top and bottom will be different. In this example, a rule of thumb (5) requires that approximately 12 linear triangles be employed to accurately resolve one complete harmonic oscillation. In the vertical direction, only four triangles were chosen since no variation of ϕ in the y direction was expected.

Figure 5 displays a comparison between the finite element calculations, shown by the solid symbols and the analytical calculation shown by the solid line. In this and all comparison figures to follow, the finite element calculation are displayed for the nodal points at upper and lower walls and at the centerline. The heading on the figures denote the respective positions.

Reasonable agreement is seen between the finite element results and the analytical curves. However, errors as high as ± 10 percent occur at selected positions. Other grid orientation to be presented will improve on this comparison. The deviation between the upper and lower nodes is a direct result of the nonsymmetric triangle pattern. A different arrangement of nodes contribute to the global "difference" equation used to calculate ϕ_j at the upper and lower surfaces for the same axial position..

Figure 6 displays similar results for the nonsymmetric grid for the hard wall exit conditions

($\partial\phi/\partial x = 0$). In this case, the errors are very large and the result not satisfactory.

The results for the nonsymmetric grid for the potential relief exit condition ($\phi = 0$) are now considered. For a wave number of zero ($k = 0$), exact agreement is obtained. The upper, center, and lower surface finite element results coincide because of the linear nature of the solution, Eq. (22). For k greater than zero ($k = \pi/2$), the results are very good and just a slight variation between the upper and lower surfaces are seen. For $k = 3\pi/2$ shown in Fig. 7, the results are totally unsatisfactory.

In order to check for convergence of the nonsymmetric grid when $k = 3\pi/2$, the vertical direction was divided into 20 elements. For this case as shown in Fig. 8, the agreement between the finite element and analytical results is good. However, the use of many elements to resolve a vertically nonvarying potential is quite unacceptable. Therefore, let us now consider some symmetric triangular grids.

Symmetric Diamond Pattern

The symmetric diamond pattern shown in Fig. 9 was used to calculate the potential relief boundary condition ($\phi = 0$, $k = 3\pi/2$) as shown in Fig. 10 and the wave propagation without reflection at the exit as displayed in Fig. 11. In Fig. 10, agreement between the finite element calculations and the analytical results are excellent, and thereby preferred over the nonsymmetric grid displayed in Fig. 4. Only the upper wall values are seen, since they are identical to the lower wall values and thus obscure the lower values. In Fig. 11 for the nonreflecting exit, some significant error is still seen at an x value of 0.5.

In practical applications, wave guides might have both vertical and horizontal laminated changes in material. To more conveniently resolve the boundary between laminated regions, some additional symmetric triangular patterns will now be considered.

Symmetric Saw Tooth Pattern

The symmetric saw tooth pattern shown in Fig. 12 was used to calculate the potential relief boundary condition ($\phi = 0$, $k = 3\pi/2$) as shown in Fig. 13. As seen in Fig. 13, excellent results are obtained. There is however, a slight variation between the center values and the wall values. Again, only the upper wall values are seen, since they are identical to the lower wall values and thus obscure the lower value.

Symmetric Pyramid Pattern

The symmetric pyramid pattern shown in Fig. 14 was used to calculate the potential relief boundary condition ($\phi = 0$, $k = 3\pi/2$) as shown in Fig. 15 and the wave propagation without reflection at the exit as displayed in Fig. 16. In both cases, agreement between the finite element calculations and the analytical results are excellent. In these cases, the values of the potential for the upper and lower walls and centerline are identical. Thus, only the upper wall data point appears in these figures. The agreement in Fig. 16 at $x = 0.5$ represents a significant improvement over the diamond pattern results of Fig. 11.

CONCLUDING REMARKS

The finite element solutions for the Helmholtz equation were presented for no reflection, hard wall, and potential relief exit terminations with a variety of triangular element orientations. Nonsymmetric element patterns were found to give generally poor results in the model problems investigated. For a fixed number of vertical elements, the results showed that symmetric element patterns give much better agreement with corresponding exact analytical results. For layered grids which may be needed for laminated wave guide applications, the symmetric pyramid pattern was found to give the best results and was very convenient to program.

REFERENCES

1. Baumeister, K.J., "Wave Envelope Analysis of Sound Propagation in Ducts with Variable Axial Impedence," Aeroacoustics: Fan Noise and Control; Duct Acoustics; Rotor Noise, Ira R. Schwartz, Henry T. Nagamatsu, and Warren Strohle, eds. AIAA Progress in Astronautics and Aeronautics Series, Vol. 44, AIAA, 1976, pp. 451-474.
2. Silvester, P.P., and Ferrari, R.L., Finite Elements for Electrical Engineers, Cambridge University Press, Cambridge, England, 1983.
3. Korczak, K.Z., and Patera, A.T., "An Isoparametric Spectral Element Method for Solution of the Navier-Stokes Equation in Complex Geometry," Journal of Computational Physics, vol. 62, no. 2, Feb. 1986.
4. Rockey, K.C., Evans, H.R., Griffiths, D.W., and Nethercot, D.A., The Finite Element Method, 2nd ed., Wiley, New York, 1983.
5. Baumeister, K.J., "Numerical Techniques in Linear Duct Acoustics - A Status Report," Journal of Engineering for Industry, vol. 103, no. 3, Aug. 1981, pp. 270-281.
6. Reynolds, D., Engineering Principles of Acoustic Noise and Vibration Control, Allyn and Bacon, Boston, 1981.
7. Dhatt, G., and Touzot, G., (G. Cantin, Transl.), The Finite Element Method Displayed, Wiley, New York, 1984.
8. Lester, H.C. and Parrott, T.L., "Application of a Finite Element Method for Computing Grazing Incidence Wave Structure in an Impedance Tube: Comparison with Experiment," AIAA paper 79-0664, Mar. 1979.
9. Unruh, J.F., "A Finite Element Subvolume Technique for Structural-Borne Interior Noise Predictions," AIAA Paper 79-0585, Mar. 1979.
10. Martin, H.C. and Carey, G.F., Introduction to Finite Element Analysis, McGraw-Hill, New York, 1973.
11. Segerlind, L.J., Applied Finite Element Analysis, Wiley, New York, 1976.
12. Patankar, S.V. and Shih, T.M., Numerical Heat Transfer and Fluid Flow, McGraw-Hill, New York, 1980.
13. Adey, R.A. and Brebbia, C.A., Basic Computational Techniques For Engineers, Wiley, New York, 1983.

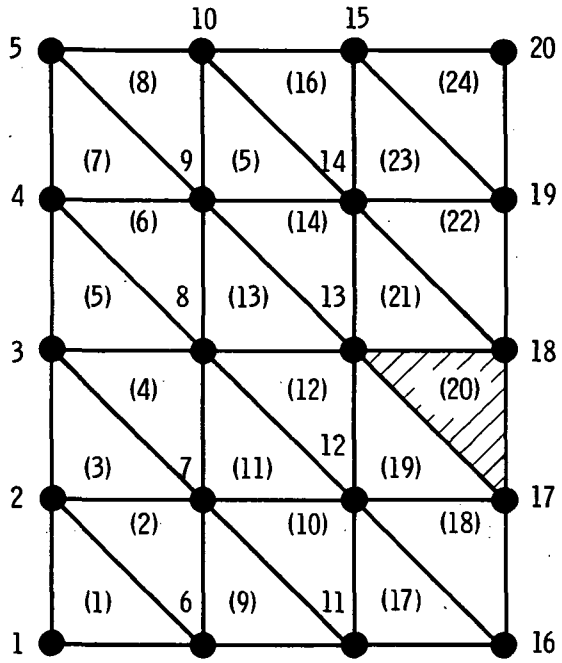

(a) Non-symmetric.

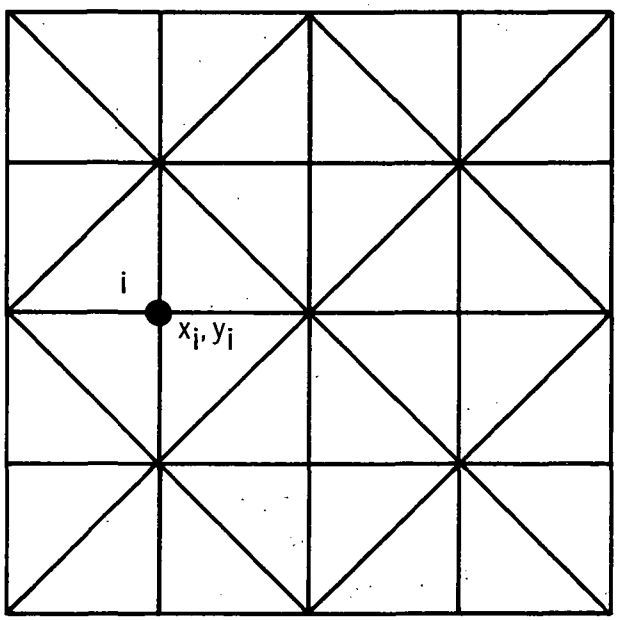

(b) Symmetric x-y directions.

Figure 1. - Linear triangular elements.

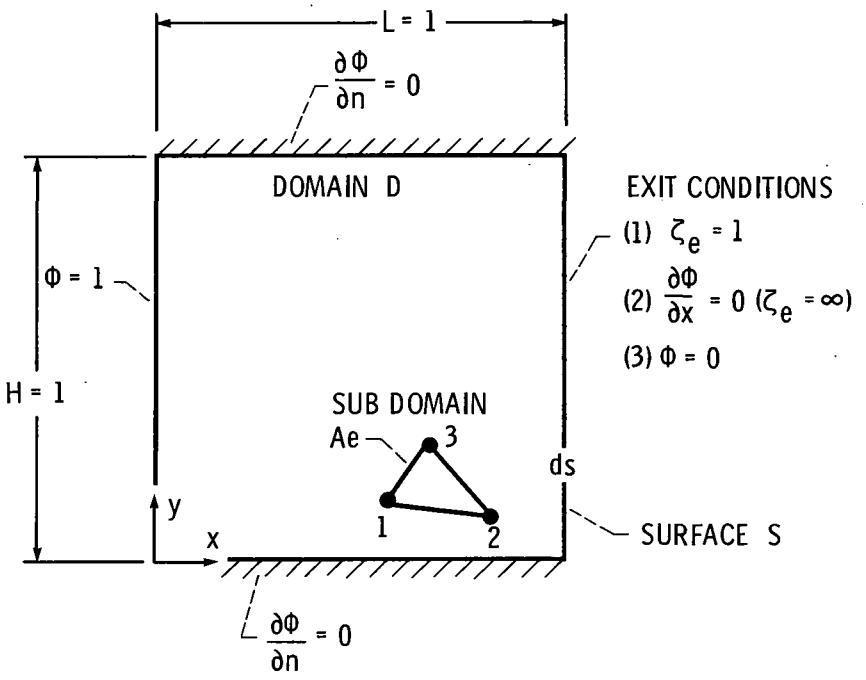

Figure 2. - Mixed boundary value problem.

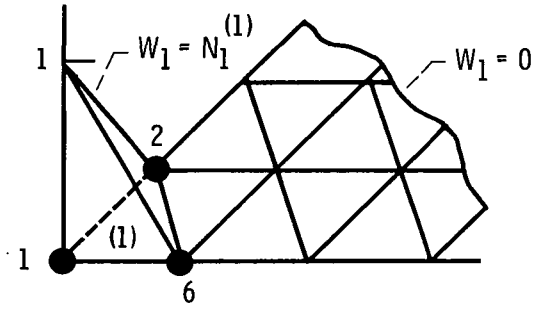

(a) $N_1^{(1)}$ Shape function.

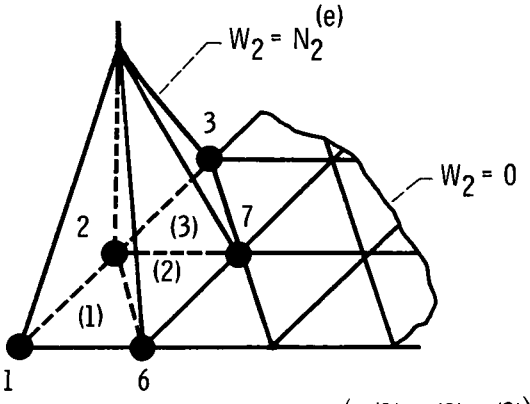

(b) N_2 Shape functions $\left(N_2^{(1)}, N_2^{(2)}, N_2^{(3)}\right)$.

Figure 3. - Finite element approximations of Global basis functions.

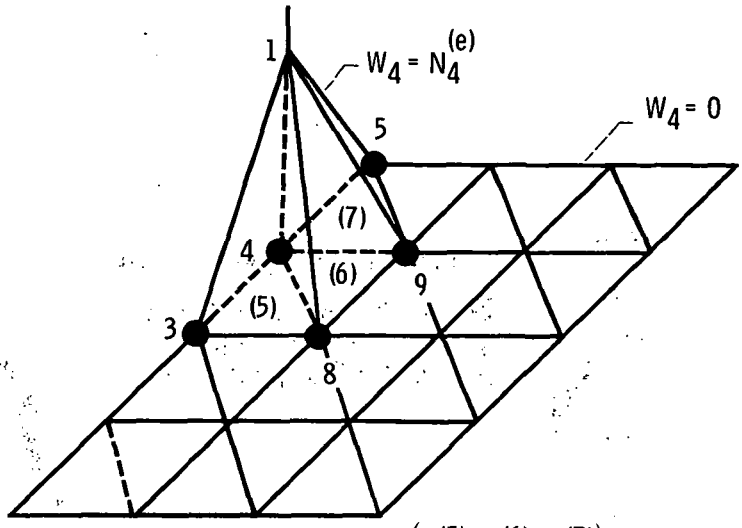

(c) N_4 Shape functions $\left(N_4^{(5)}, N_4^{(6)}, N_4^{(7)}\right)$.

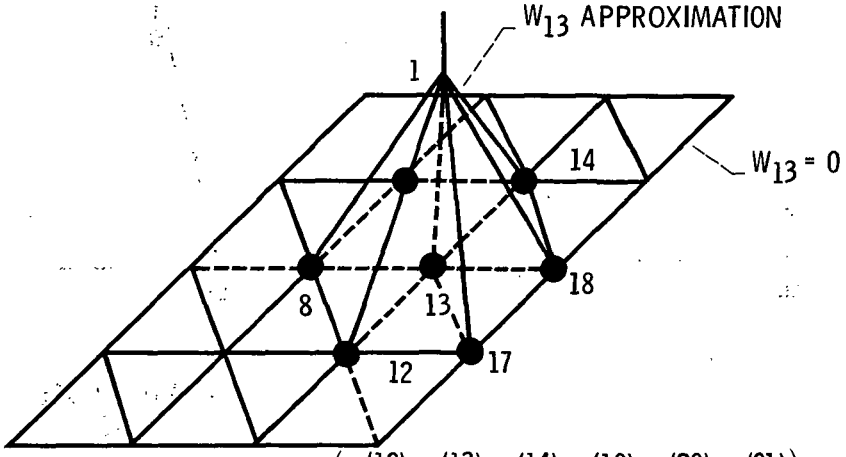

(d) N_{13} Shape functions $\left(N_{13}^{(12)}, N_{13}^{(13)}, N_{13}^{(14)}, N_{13}^{(19)}, N_{13}^{(20)}, N_{13}^{(21)}\right)$.

Figure 3. - Concluded.

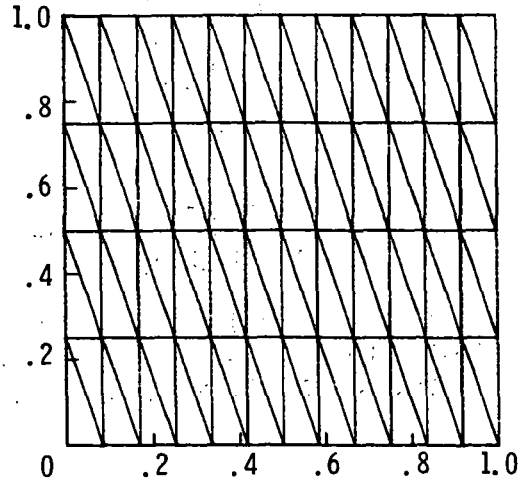

Figure 4. - Discretization of solution domain using non-symmetric triangles for $k = 2\pi$, $\zeta_e = 1.0$, $\Delta X = 0.083$ and 5 vertical nodes.

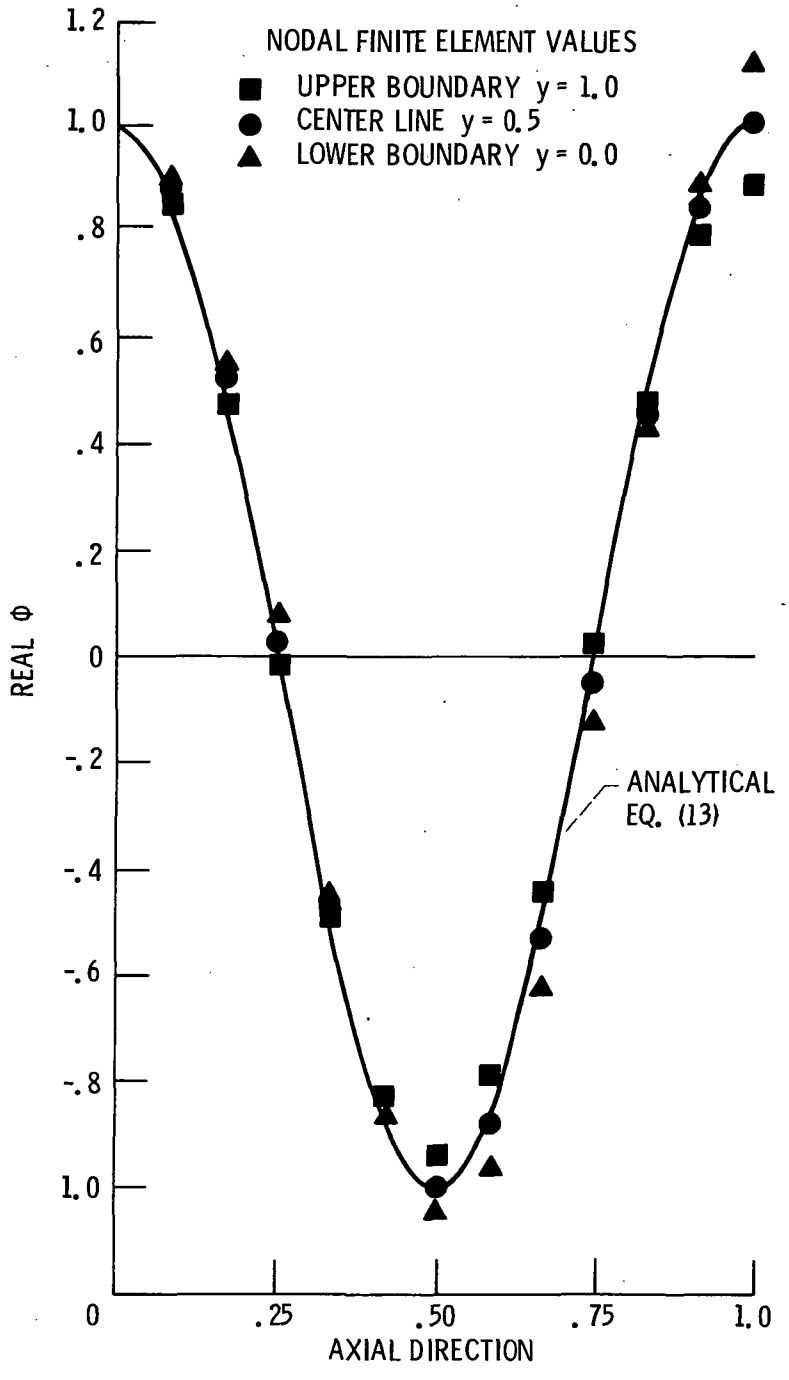

Figure 5. - Potential Φ profile using non-symmetric discretization for $k = 2\pi$ and $\Delta X = 0.083$ with non-reflecting exit, $\zeta_e = 1$ and 5 vertical nodes.

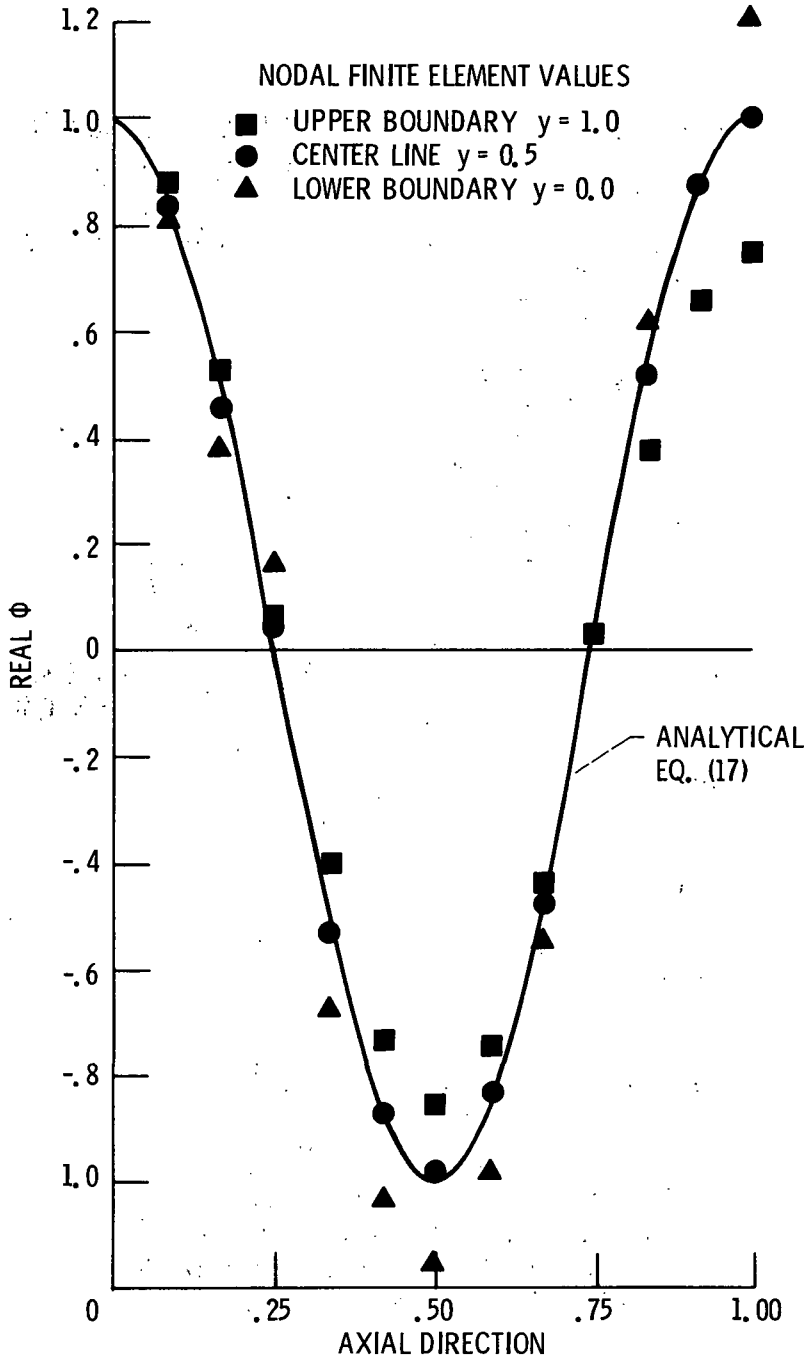

Figure 6. - Potential Φ profile using non-symmetric discretization for $k = 2\pi$ and $\Delta X = 0.083$ with 5 vertical nodes and hard wall exit $(\partial\Phi/\partial x = 0$.

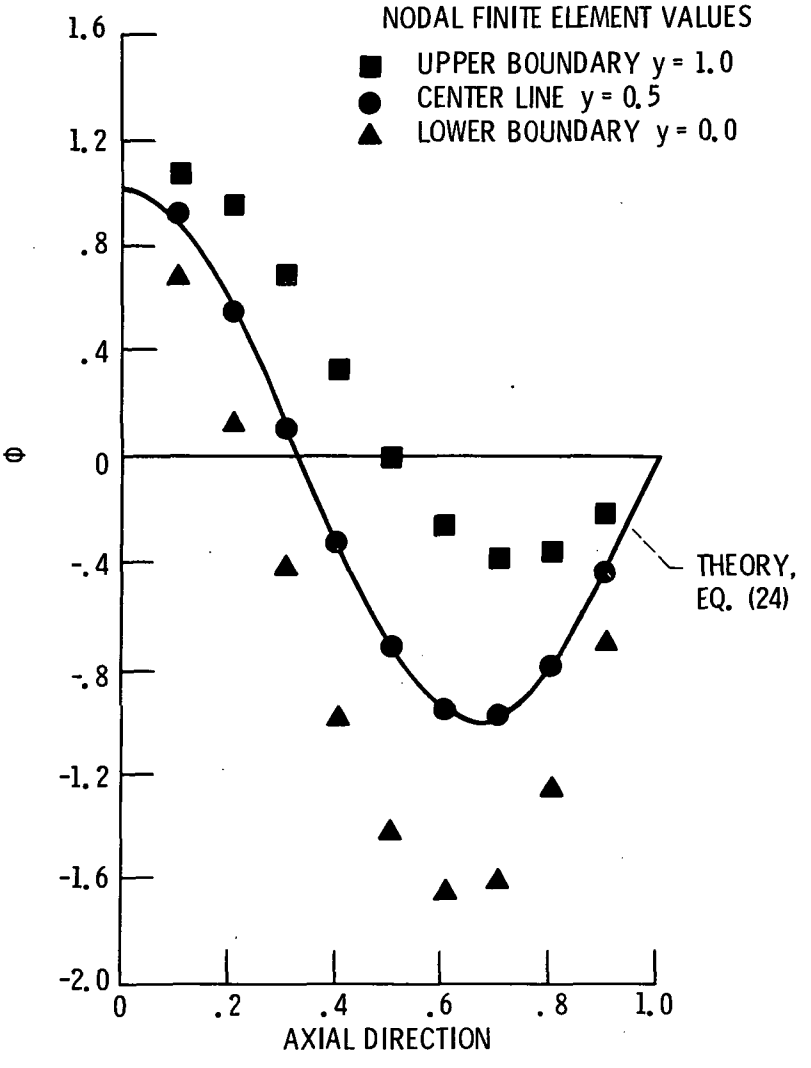

Figure 7. - Potential Φ profile using non-symmetric discretization for dimensionless wave number $k = 3\pi/2$ with 5 vertical nodes and $\Delta x = 0.1$ with $\Phi = 0$ at exit.

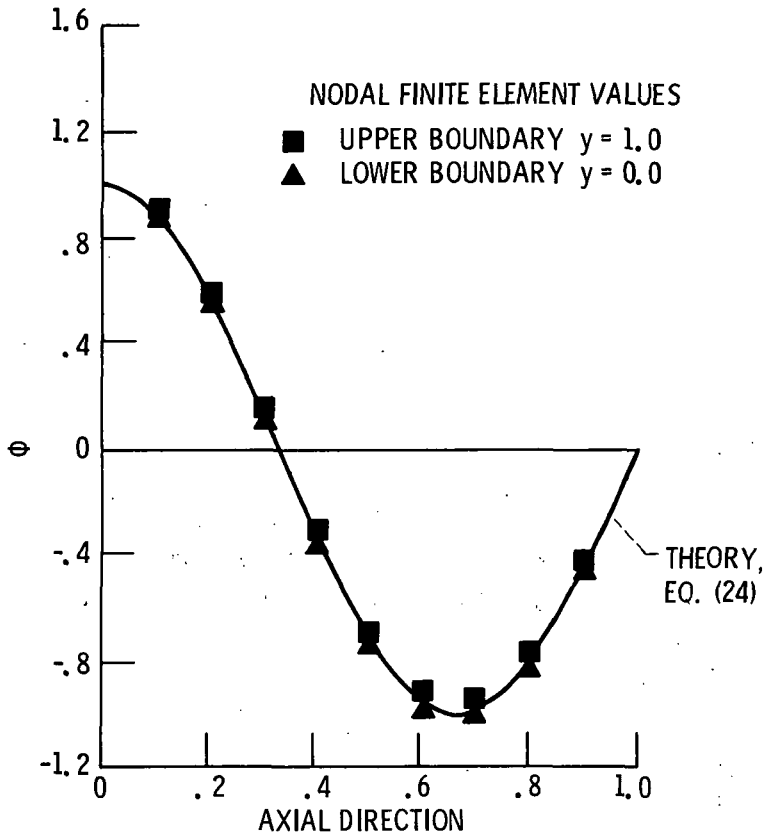

Figure 8. - Potential Φ profile using non-symmetric discretization for dimensionless wave number $k = 3\pi/2$ with 20 vertical nodes, $\Delta x = 0.1$ and $\Phi = 0.0$ at exit.

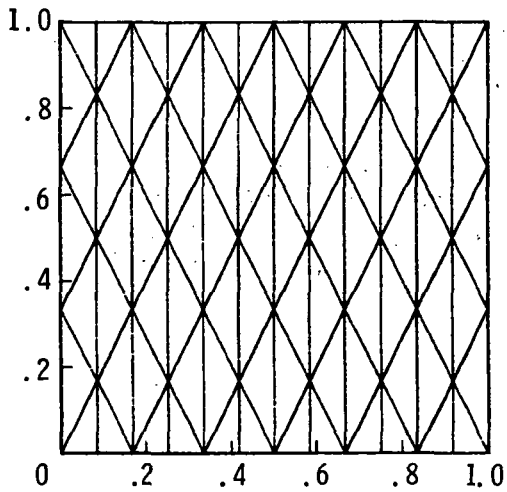

Figure 9. - Discretization of solution domain using symmetric diamond pattern for $k = 2\pi$ and $\Delta x = 0.083$ with 5 vertical nodes (symmetric x-y direction).

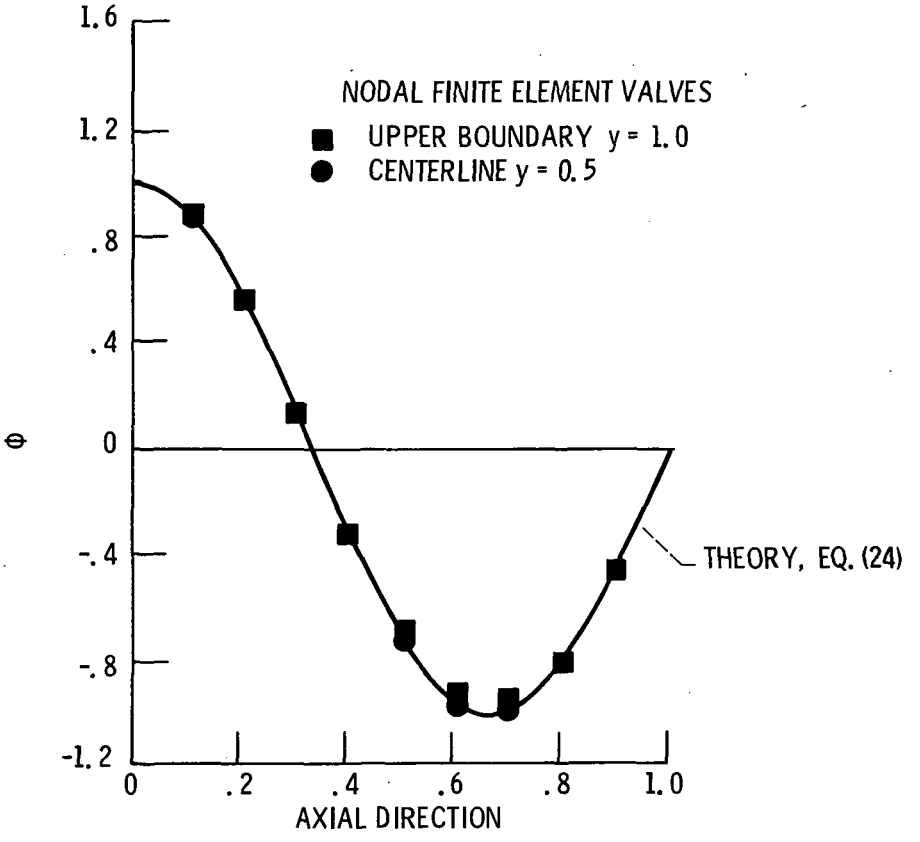

Figure 10. - Potential Φ profile using symmetric diamond discretization for dimensionless wave number $k = 3\pi/2$ with 4 vertical nodes, $\Delta x = 0.1$ and $\Phi = 0$ at exit.

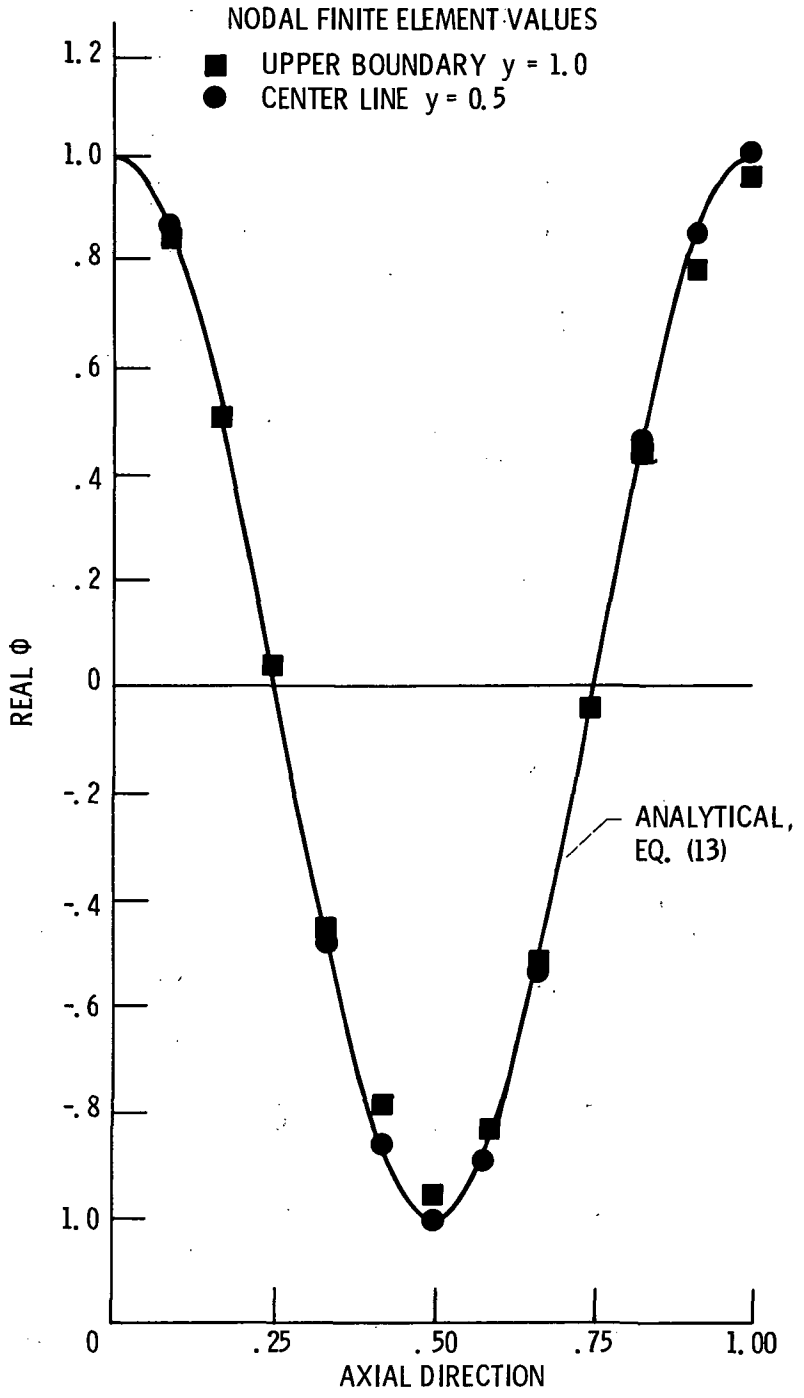

Figure 11. - Potential Φ profile using symmetric diamond discretization for $k = 2\pi$ and $\Delta x = 0.083$ with non-reflecting exit, $\zeta_e = 1$.

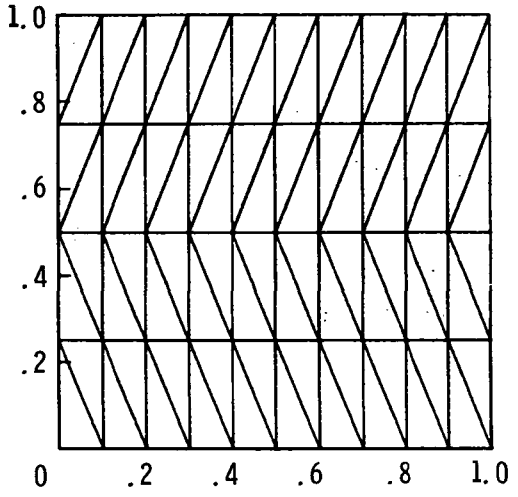

Figure 12. - Discretization of solution domain using symmetric saw tooth pattern for $k = 3\pi/2$ and $\Delta x = 0.1$ with 5 vertical nodes. (Symmetric y-direction.)

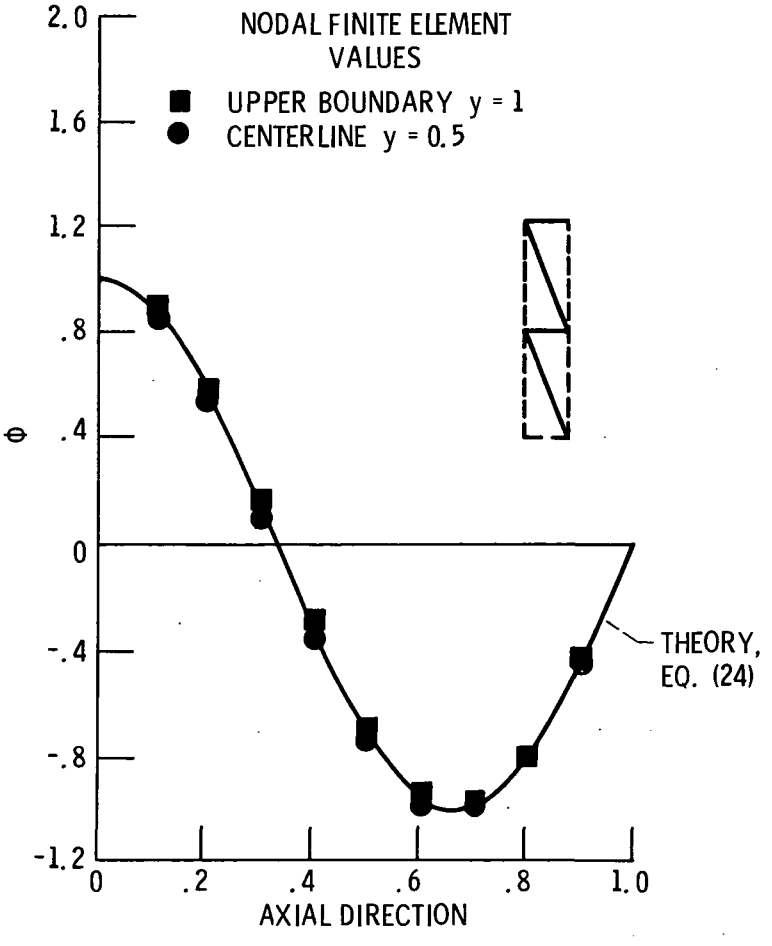

Figure 13. - Potential Φ profile using saw tooth discretization for dimensionless wave number $k = 3\pi/2$ with 5 vertical nodes, $\Delta x = 0.1$ and $\Phi = 0$ at exit.

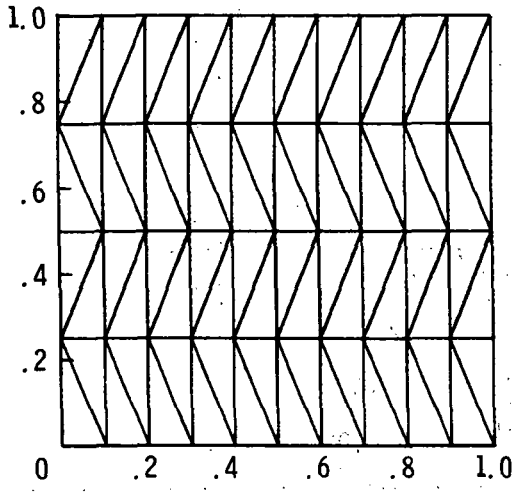

Figure 14. - Discretization of solution domain using symmetric pyramid pattern for $k = 3\pi/2$ and $\Delta x = 0.1$ with 5 vertical nodes. (Symmetric y-direction.)

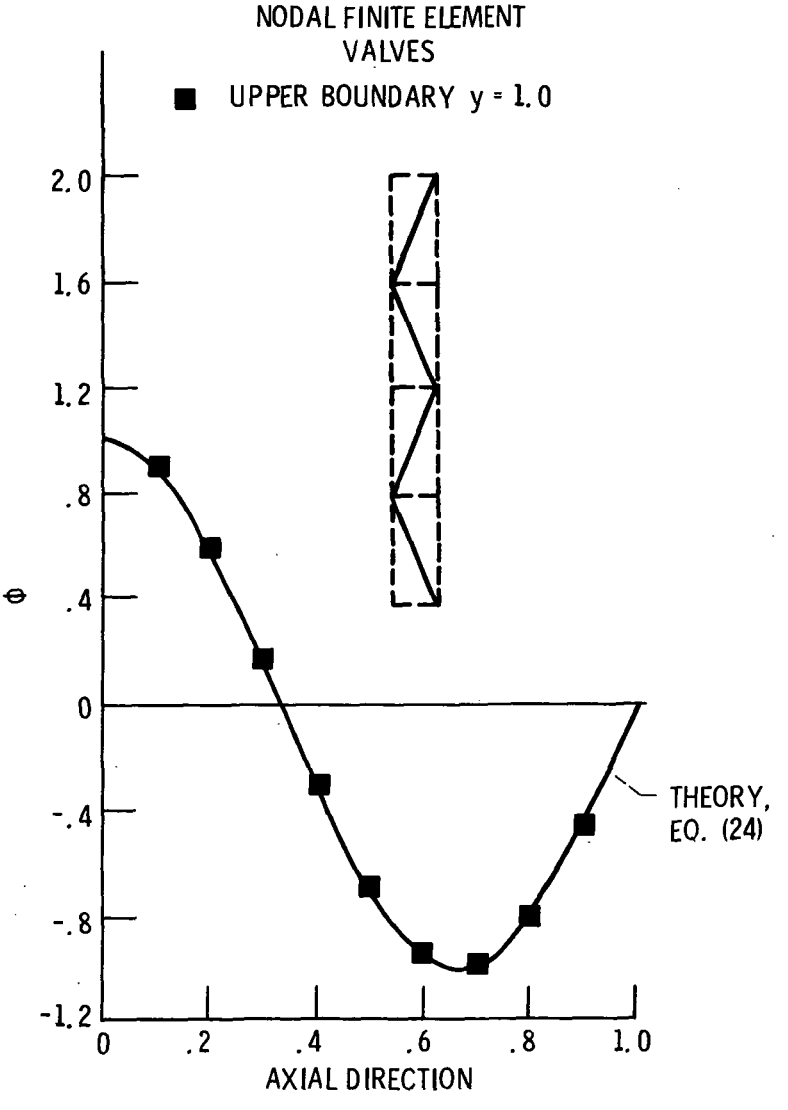

Figure 15. - Potential Φ profile using symmetric pyramid discretization for dimensionless wave number $k = 3\pi/2$ with 5 vertical nodes, $\Delta x = 0.1$ and $\Phi = 0$ at exit.

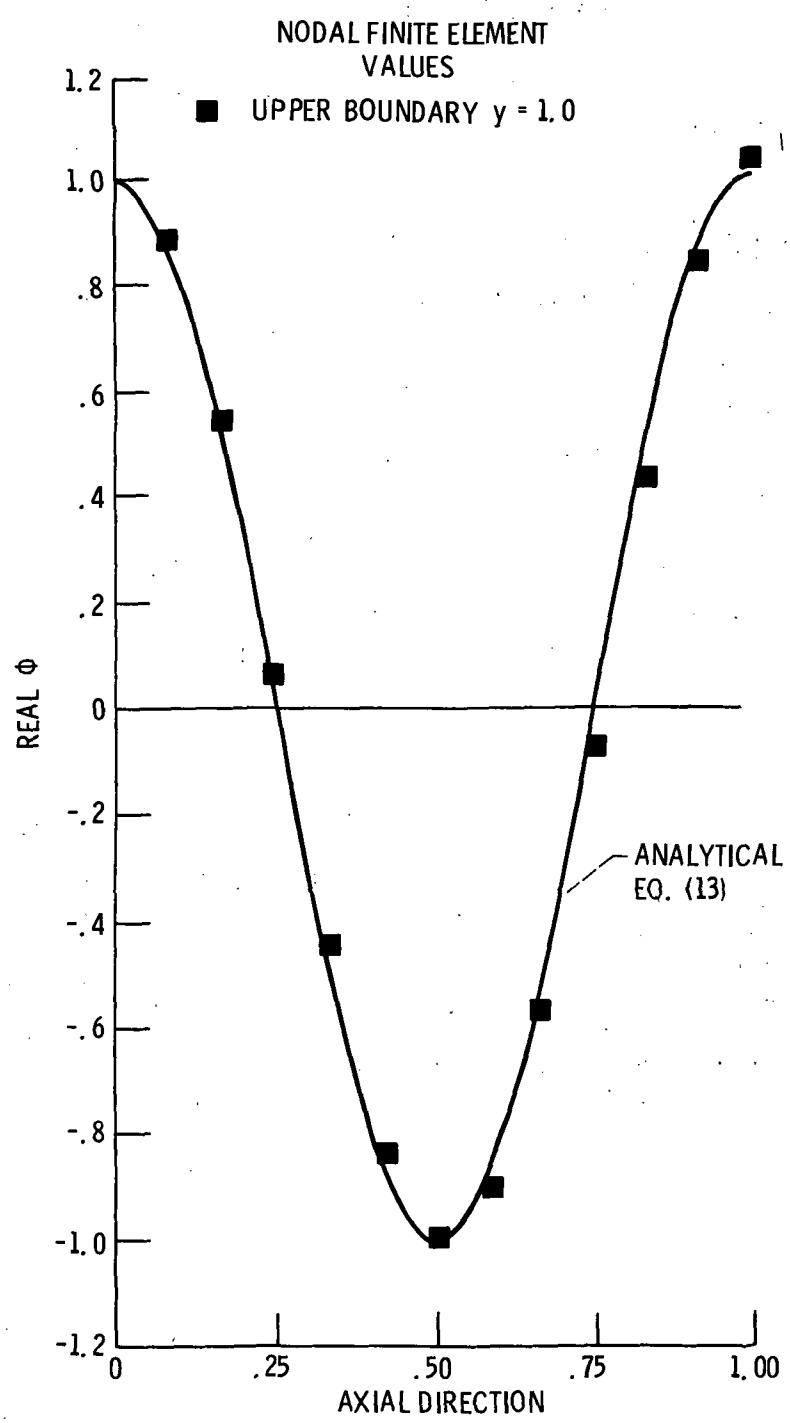

Figure 16. - Potential Φ profile using symmetric pyramid discretization for $k = 2\pi$ and $\Delta x = 0.083$ with non-reflecting exit, $\zeta_e = 1$ and 5 vertical nodes.

1. Report No.	2. Government Accession No.	3. Recipient's Catalog No.
NASA TM-87351		

4. Title and Subtitle	5. Report Date
Effect of Triangular Element Orientation on Finite Element Solutions of the Helmholtz Equation	6. Performing Organization Code: 505-62-21
7. Author(s): Kenneth J. Baumeister	8. Performing Organization Report No.: E-2734
	10. Work Unit No.
9. Performing Organization Name and Address: National Aeronautics and Space Administration, Lewis Research Center, Cleveland, Ohio 44135	11. Contract or Grant No.
	13. Type of Report and Period Covered: Technical Memorandum
12. Sponsoring Agency Name and Address: National Aeronautics and Space Administration, Washington, D.C. 20546	14. Sponsoring Agency Code

15. Supplementary Notes

Prepared for the 1986 Winter Annual Meeting of the American Society of Mechanical Engineers, Anaheim, California, December 7-12, 1986.

16. Abstract

The Galerkin finite element solutions for the scalar homogeneous Helmholtz equation are presented for no reflection, hard wall, and potential relief exit terminations with a variety of triangular element orientations. For this group of problems, the correlation between the accuracy of the solution and the orientation of the linear triangle is examined. Nonsymmetric element patterns are found to give generally poor results in the model problems investigated, particularly for cases where standing waves exist. For a fixed number of vertical elements, the results showed that symmetric element patterns give much better agreement with corresponding exact analytical results. In laminated wave guide application, the symmetric pyramid pattern is convenient to use and is shown to give excellent results.

17. Key Words (Suggested by Author(s))	18. Distribution Statement
Finite elements, Helmholtz equation, Triangles	Unclassified - unlimited STAR Category 71

19. Security Classif. (of this report)	20. Security Classif. (of this page)	21. No. of pages	22. Price*
Unclassified	Unclassified		

*For sale by the National Technical Information Service, Springfield, Virginia 22161

National Aeronautics and
Space Administration

Lewis Research Center
Cleveland, Ohio 44135

SECOND CLASS MAIL

ADDRESS CORRECTION REQUESTED

Official Business
Penalty for Private Use $300

Postage and Fees Paid
National Aeronautics and
Space Administration
NASA-451

NASA